Composites: Part A 40 (2009) 1248–1256

Contents lists available at ScienceDirect

Composites: Part A

journal homepage: www.elsevier.com/locate/compositesa

Crush energy absorption of composite channel section specimens

Paolo Feraboli [a,*], Bonnie Wade [a], Francesco Deleo [a], Mostafa Rassaian [b]

[a] Department of Aeronautics and Astronautics, University of Washington, Seattle, WA, United States
[b] Advanced Structures Technology, Boeing Phantom Works, Seattle, WA, United States

ARTICLE INFO

Article history:
Received 25 February 2009
Accepted 21 May 2009

Keywords:
A. Carbon fibre
B. Fragmentation
B. Impact behavior
D. Mechanical testing

ABSTRACT

Carbon/epoxy square tubes and channel sections have been used in modern automotive and aircraft structures, respectively, as dedicated components designed to dissipate energy under controlled collapse. However, there are currently no specialized test methods for the characterization of Specific Energy Absorption (SEA) of composite materials. A systematic experimental investigation is conducted to evaluate the effect of geometric features on crush behavior. From a square tube, individual test segments are machined in order to isolate corner radii and flat sections of varying sizes, for a total of five different test geometries. Laminate thickness, material system, manufacturing process, and test methodology are kept constant throughout the study. For the material system and lay-up considered in this study, fiber tensile fracture and tearing at the corners is responsible for the vast percentage of the energy absorbed, while frond formation and splaying of the flat segments is responsible for a much lower percentage. An analytical expression is derived that accounts for the combined behavior of corner elements and flat segments in the crush behavior of more complex test articles, such as tubes.

1. Introduction

The energy-absorbing behavior of composites is not easily predicted due to the complexity of the failure mechanisms that can occur within the material. Composite structures fail through a combination of fracture mechanisms, which involve fiber fracture, matrix cracking, fiber–matrix debonding, and delamination [1]. The brittle failure modes of many polymeric composite materials can make the design of energy-absorbing crushable structures difficult. Furthermore, the overall response is highly dependent on a number of parameters, including the geometry of the structure, material system, lay-up, and impact velocity.

Tubular structures are used by the motorsport and automotive industries as dedicated members to absorb energy in the event of a crash, including automotive-sized front rails (Fig. 1). Prepreg or fabric can easily be formed to tubular shapes and is the material of choice for the motorsport industry. Although no standard shape or dimension exists, either circular or square tubes have been traditionally employed, the latter having rounded corners [2].

The vast majority of the research conducted to determine the crush energy absorption of composite materials has focused on thin-wall tubular specimens [1–3]. Only a limited number of attempts have used test specimens of different geometries, and have included both self-supporting shapes, such as semicircular segments [4], channel stiffeners [5], corrugated webs [6], as well as flat plate specimens with dedicated anti-buckling fixtures [7]. The history behind the selection of tubular specimens can be attributed to several reasons: they are self-supporting, they do not require dedicated test fixtures, and they are ideally suited for both quasi-static and dynamic crushing.

The use of tubular specimens however poses several challenges for novel material forms and processes, including liquid resin infusion or resin transfer molding, as well as compression molding. Furthermore, it has been shown that the closed-section nature of tubes has unknown but evident effects on the crush performance. In particular, it is thought that stacking sequence affects the crush behavior, since the hoop fibers constrain the axial fibers and prevent them from splaying, thereby suppressing the propagation of the crash front.

The aerospace community has focused mostly on test specimens that resemble subfloor structures, such as floor beams, longerons, stanchions and stiffeners. These typically exhibit either a corrugated or channel shape, which are open section and are partially self-supporting, and therefore do not require a dedicated test fixture. They are therefore more versatile from a manufacturing standpoint, and do not exhibit the hoop fiber constraint as tubular shapes. Bolukbasi and Laananen [5] conducted a systematic comparison of three structural configurations. Flat plates, angle sections, and C-channels were crushed under quasi-static conditions (Fig. 2). Unidirectional tape was the material used, and two different lay-ups were considered. The NASA fixture described in [8,9]

* Corresponding author. Address: Department of Aeronautics and Astronautics, University of Washington, Guggenheim Hall Box 352400, Seattle, WA 98195-2400, United States. Tel.: +1 206 543 2170; fax: +1 206 543 0217.
E-mail address: feraboli@u.washington.edu (P. Feraboli).

1359-835X/$ - see front matter © 2009 Elsevier Ltd. All rights reserved.
doi:10.1016/j.compositesa.2009.05.021

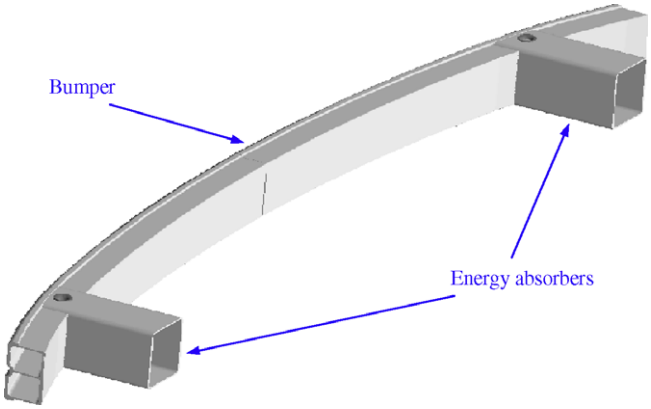

Fig. 1. Example of typical bumper beam and tubular front rail assembly [2].

was used to provide anti-buckling support for the plate specimen. Although the number of specimens tested was limited, as was the selection of laminate lay-ups, it was found that the flat plates tested with the NASA fixture yielded higher Specific Energy Absorption (SEA) measurements than any of the self-supporting specimens, mostly attributable to the overly-constrained nature of the specimen. It was also shown that for both lay-ups tested, corner stiffeners yielded lower SEA than C-channel sections.

The purpose of this study is to identify the effect of cross-section geometry on the overall crush behavior of five different specimen shapes, which are all obtained starting from a square tube with rounded corners (Fig. 3). These include a small and a large C-channel element, and a small and a large corner element, as well as the square tube itself. The ultimate goal is to isolate the SEA contribution of the corner detail from the total SEA of the section tested. This is achieved by varying the length of the flat segments among the different shapes and then extrapolating the effective, or in situ, SEA associated to the flat segments. To verify the predictions, a limited set of crush tests is performed with the flat plate specimens and modified NASA fixture proposed by the authors in [7].

2. Experimental setup

The material system is T700/2510 carbon fiber/epoxy prepreg, supplied by Toray Composites of America. It is a flat woven, 12 k tow, plain weave fabric with a 270° F cure resin (132 °C) designated for vacuum bag and oven cure only. The lay-up considered is $[0/90]_{4s}$, yielding an average cured laminate thickness t of 0.065 in. (1.65 mm). This material is used extensively for general aviation primary structures, and its properties are well documented as part of the FAA-sponsored AGATE Program (Advanced General Aviation Transport Experiment [10]). These properties are now available in the CMH-17 database [11]. Flat panels as well as tubular shapes are manufactured by the material supplier, Toray Composites of America.

Using an aluminum square tubular mandrel, the square tube is extracted from the mold. After trimming, the length of the specimen is 3.5 in. (88.9 mm). The radius of the mandrel, and hence the inner radius r of the tube, is 0.175 in. (4.45 mm). The cross-section of the tube has outer dimensions $L1 \times L1$ (Fig. 3, I) and a total perimeter of S_I (Fig. 4, I). In order to obtain the other four shapes

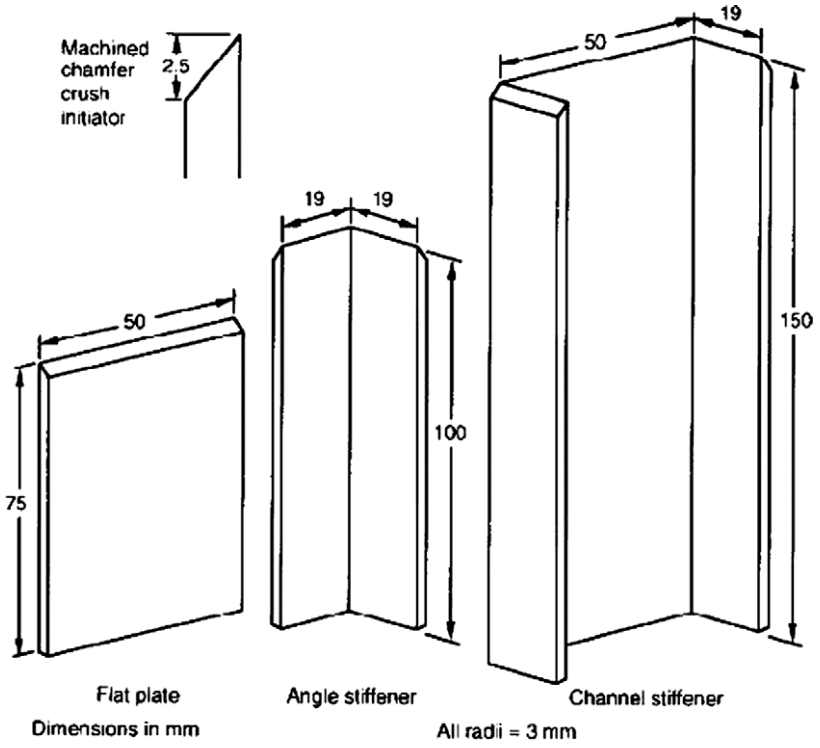

Lay-up	Flat	Angle	C-channel
$[45]_{10}$	89	54	68
$[45_2/0_2/45_2]_s$	96	67	83

Fig. 2. Comparison of specimen geometry on the measured SEA [5] in J/g for two different unidirectional tape stacking sequences.

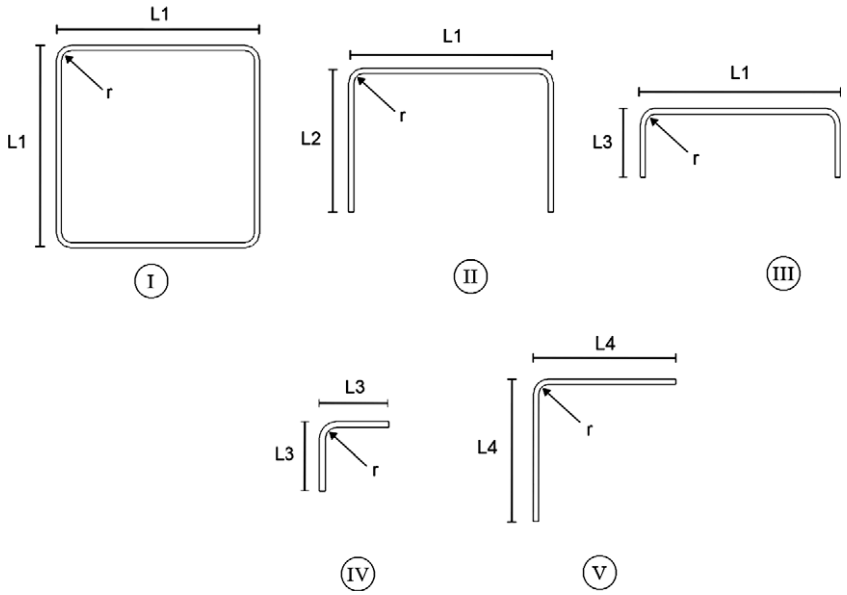

Fig. 3. Sketch of cross-section shape and dimensions for all five specimens considered.

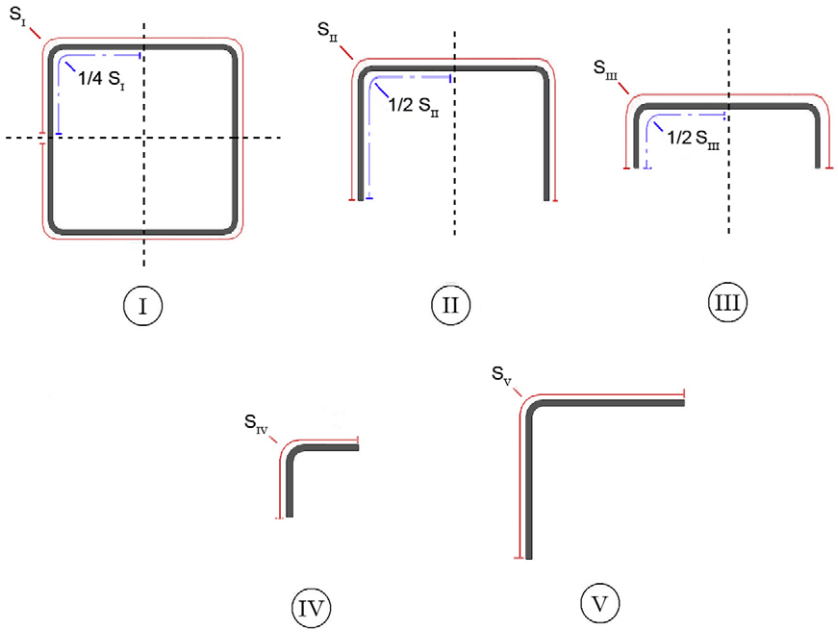

Fig. 4. Illustration of the concept of section length for each geometry considered, and portion of such length influenced by a single corner detail.

considered in this study, a portion of the square tube specimens are cut with a diamond-coated disk saw. With a single cut performed off-axis on the square cross-section (Fig. 5, I) the large and the small C-channel sections are obtained (Fig. 5, II and III, respectively). The large C-section has dimensions $L1 \times L2$, while the small C-channel has outer dimensions $L1 \times L3$, where $L3$ is the given by $L1–L2$ (Fig. 3, II and III). The total perimeters for the large and small C-channels are indicated as S_{II} and S_{III}, respectively (Fig. 4, II and III). In order to obtain the fourth specimen, a second cut is performed on a portion of the small C-channels previously obtained. The cut is performed off-axis (Fig. 5, IV), and it enables for isolating a single corner element. The small corner element has outer dimensions $L3 \times L3$ (Fig. 3, IV), and a perimeter indicated by S_{IV} (Fig. 4, IV). The fifth and last specimen, the large corner element, is obtained by performing two cuts on the original square section I (Fig. 5, V), in the proximity of two opposing corners. The specimen has outer dimension $L4 \times L4$ (Fig. 3, V), and section length S_V (Fig. 4, V). Tables 1 and 2 show in detail the list of parameters introduced and the associated numerical values.

Each of the five sections considered in this study is comprised of one or more corner details, and additional segments of flat material. If the small corner detail, specimen IV, is used as the repetitive unit, each cross-section can be subdivided into half- or quarter-sections that are influenced by a single corner detail. The purpose of this effort is to be able to measure the SEA and crush behavior of a stand-alone corner element, and then extrapolate the actual in situ SEA and crush behavior of the flat sections, which is otherwise difficult to assess experimentally [7–9].

To that extent, the square tube cross-section can be subdivided in a quarter-section, comprised of the corner detail of perimeter

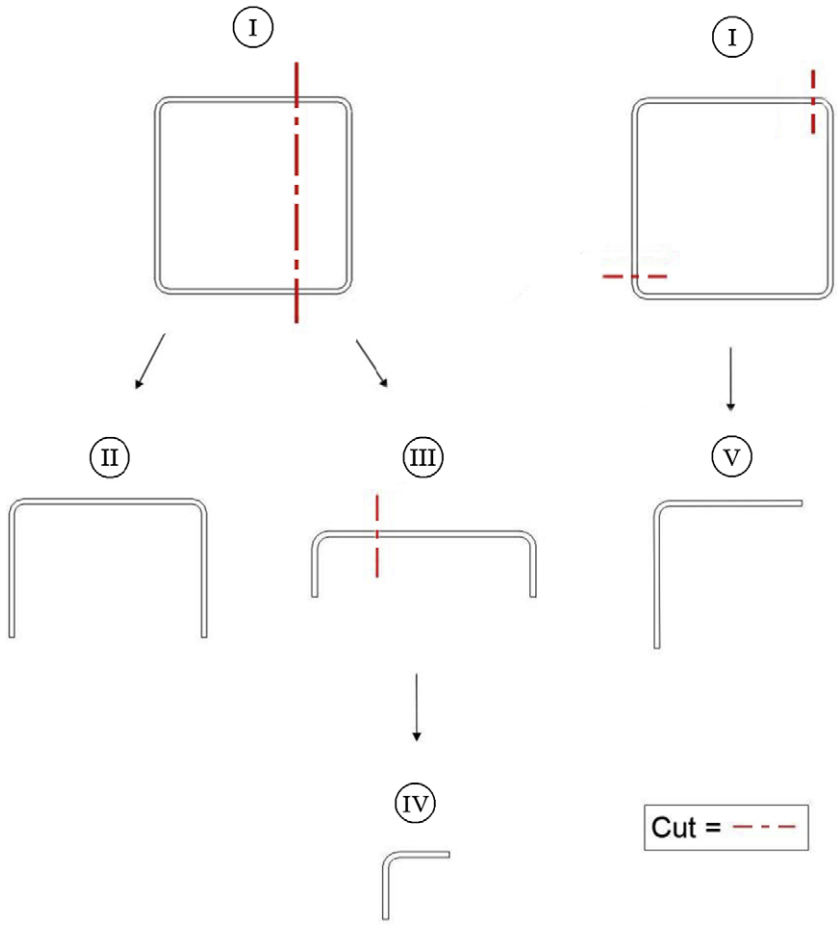

Fig. 5. Shematic of machining operation performed to obtain test specimens II–V beginning from specimen I.

Table 1
Summary of the five specimens considered and associated key geometric features.

Specimen no.	Shape	Outer dimensions	Section length	Portion of cross-section affected by one corner
I	Tube	$L1 \times L1$	S_I	$\frac{1}{4}S_I$
II	Large channel	$L1 \times L2$	S_{II}	$\frac{1}{2}S_{II}$
III	Small channel	$L1 \times L3$	S_{III}	$\frac{1}{2}S_{III}$
IV	Small corner	$L3 \times L3$	S_{IV}	S_{IV}
V	Large corner	$L4 \times L4$	S_V	S_V

S_{IV}, and two additional flat segments on both sides of the corner, each of length $\Delta S'$ (Fig. 6, I). This quarter section represents the portion of the square cross-section that is influenced by a single corner detail, since the double symmetry accounts for the other three corner elements.

For the large C-channel, the half-section comprises the corner detail of perimeter S_{IV}, same as the corner element specimen, and two additional flat segment of total length $\Delta S'$ and $\Delta S''$ (Fig. 6, II). This half section represents the portion of the large C-channel cross-section that is influenced by a single corner detail, since symmetry accounts for the other corner element.

Similarly, the small C-channel can be subdivided into a half-section, comprised of the corner detail of perimeter S_{IV}, same as the corner element specimen, and one additional flat segment of length $\Delta S'$ (Fig. 6, III).

Lastly, the large corner element can be also subdivided into a small corner element of perimeter S_{IV}, and two additional flat segments, each of length $\Delta S'''$ (Fig. 6, V).

Table 2
Summary of parameters and associated numerical values used in this study.

Parameter	Value
$L1$	2.50 in. (63.5 mm)
$L2$	1.75 in. (44.5 mm)
$L3$	0.75 in. (19.0 mm)
$L4$	2.00 in. (50.8 mm)
r	0.175 in. (4.45 mm)
t	0.065 in. (1.65 mm)
S_I	10.50 in. (266.7 mm)
S_{II}	5.75 in. (146.0 mm)
S_{III}	3.75 in. (95.3 mm)
S_{IV}	1.25 in. (31.75 mm)
S_V	4.50 in. (114.3 mm)
$\Delta S'$	0.75 in. (19.0 mm)
$\Delta S''$	1.00 in. (25.4 mm)
$\Delta S'''$	1.60 in. (40.6 mm)
ρ	1.52 g/cm^3

For each of the specimens (Figs. 4 and 6), the length of the cross-section influenced by a single corner (S_i) is defined as:

$$S_i = \begin{Bmatrix} \frac{1}{4}S_I & \text{for specimen I} \\ \frac{1}{2}S_{II} & \text{for specimen II} \\ \frac{1}{2}S_{III} & \text{for specimen III} \\ S_{IV} & \text{for specimen IV} \\ S_V & \text{for specimen V} \end{Bmatrix} \quad (1)$$

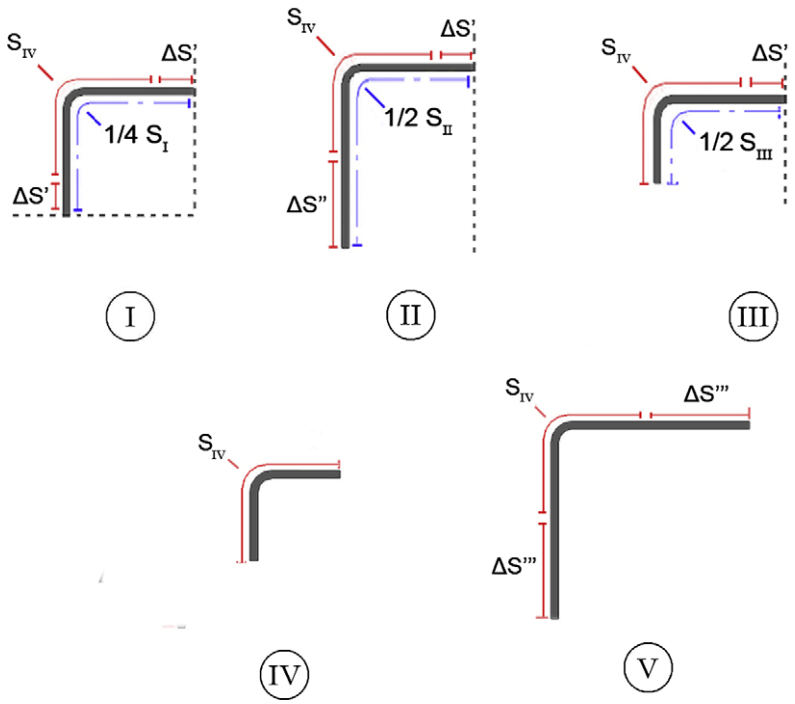

Fig. 6. Subdivision of section length into a corner detail and portion of flat segments, for each of the five specimen cross-section geometries considered.

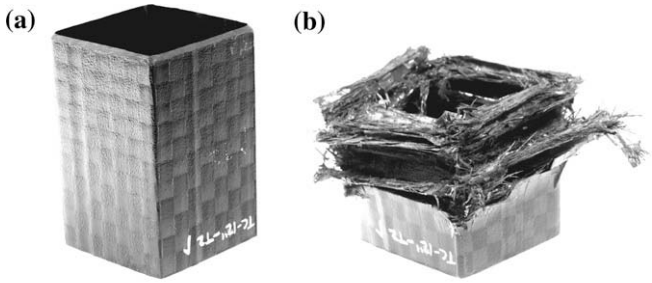

Fig. 7. (a, b) Square tube, specimen I, before and after crush testing.

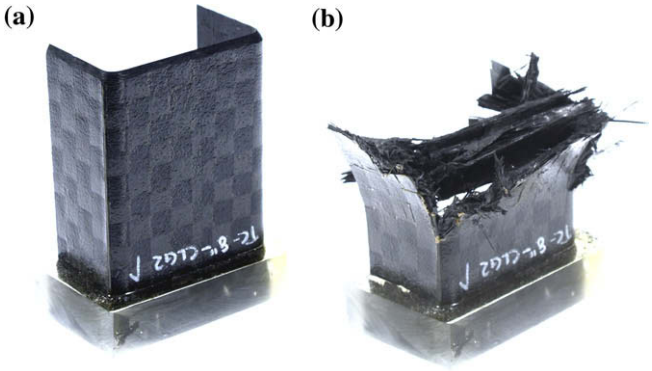

Fig. 8. (a, b) Large C-channel, specimen II, before and after crush testing.

The remaining portion of the cross-section is comprised of flat segments (Fig. 6), which are defined as:

$$\Delta S = S_i - S_{IV} \tag{2}$$

where:

$$\Delta S = \left\{ \begin{array}{cc} 2\Delta S' & \text{for specimen I} \\ \Delta S' + \Delta S'' & \text{for specimen II} \\ \Delta S' & \text{for specimen III} \\ 0 & \text{for specimen IV} \\ 2\Delta S''' & \text{for specimen V} \end{array} \right\} \tag{3}$$

Numerical values for all the quantities reported in Eqs. (2) and (3) are summarized in Table 2. The coupons are 3.5 in. long (88.9 mm), and their width varies according to geometry. The trigger is 45° single chamfer on the outside edge, as used in most studies to initiate crushing in self-stabilizing structures. All tests are conducted at a quasi-static rate of 2.0 in./min (50.8 mm/min), which is noticeably below any dynamic effect previously reported for modern systems [1,6], approximately 40 in./s (1.0 m/s). Specimens rest on a polished hardened steel surface. All section specimens except for the tube are potted into an epoxy resin base in order to provide stability during crushing; hence their effective length is reduced by at least 0.5 in. (12.5 mm). Pictures of the test specimens before and after crushing are shown in Figs. 7–11.

Flat panels are used for obtaining flat plate test specimens to be crushed using a purposely-designated fixture introduced in [7]. This fixture is an evolution of the NASA fixture [8,9], but unlike its predecessor it allows for a variable region of unsupported specimen height. This region, which is defined by the distance between the end of the knife-edge supports and the base plate, is shown in Fig. 12. The modified fixture enables the specimen to deform in a natural fashion by allowing the fronds to bend freely, and also prevents accumulation of a debris wedge between the knife-edges. The unsupported distance can be varied between 0 and 1.0 in. (0 and 25.4 mm, respectively), with intermediate values at 0.125, 0.25, 0.5, and 0.75 in. (3.2, 6.3, 12.7, 19.0, and 25.4 mm), and is achieved by moving the two sets of knife-edges up or down from the base-plate. For 0-in. (0 mm) unsupported height, the fixture is virtually equivalent to the original NASA fixture, thus providing a fully constrained specimen. The flat coupon is 3.0 in. long

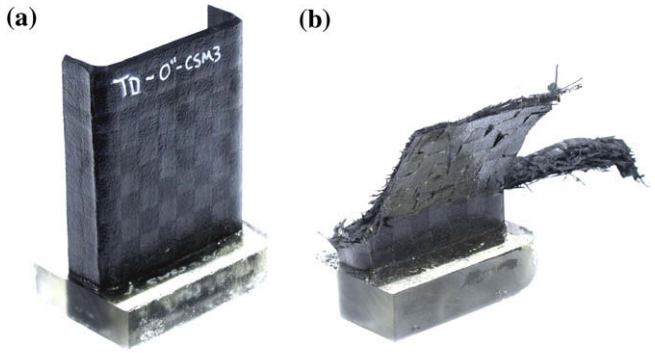

Fig. 9. (a, b) Small C-channel, specimen III, before and after crush testing.

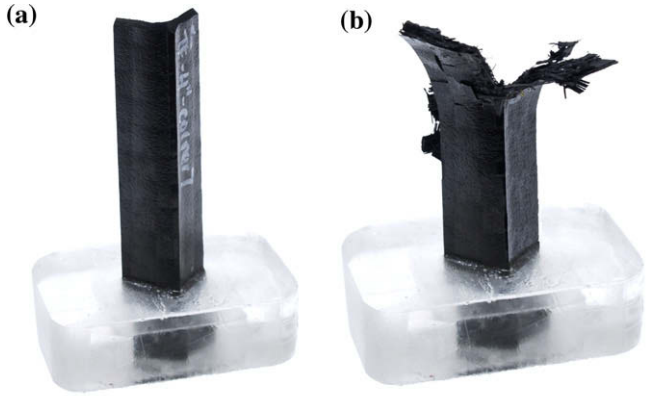

Fig. 10. (a, b) Small corner element, specimen IV, before and after crush testing.

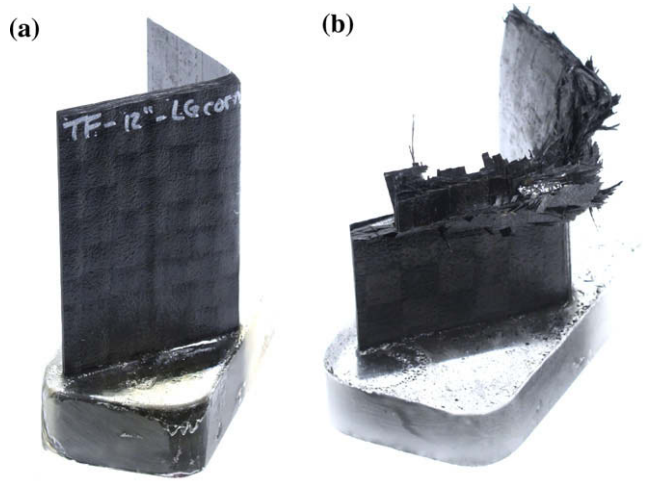

Fig. 11. (a, b) Large corner element, specimen V, before and after crush testing.

(76.2 mm) and 2.0 in. wide (50.80 mm), identical to the original NASA specimen. The trigger used is a planar saw-tooth since the single chamfer does not lead to stable crushing for flat specimens, as discussed in [7–9].

3. Results

When analyzing the energy absorption behavior of a structure, a few key definitions are required:

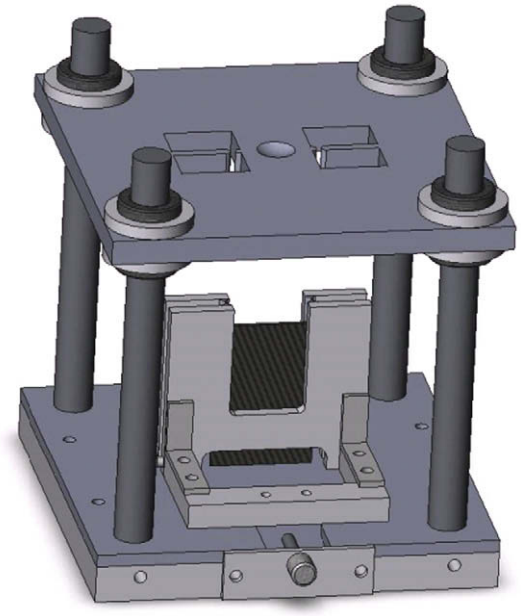

Fig. 12. Fixture developed in [7] by the authors to test flat specimens, showing 0.25 in. (6.3 mm) unsupported height.

- Peak Force, the maximum point on the Force–Stroke diagram (indicated as F^{max}).
- Average Crush Force. Also referred to as Sustained Crush Force, is the displacement-average value of the force history (indicated as F^{avg}).
- Crush efficiency – ratio of peak force to average crush force.
- Stroke. Also referred to as crush or displacement, is the length of structure/material being sacrificed during crushing (indicated as l).
- Energy absorbed. Total area under the Force–Stroke diagram (indicated as EA).
- Specific energy absorption. The energy absorbed per unit mass of crushed structure (indicated as SEA).

The ability of a material to dissipate energy can then be expressed in terms of SEA, which has units of J/g, and indicates a number, which for composites is usually comprised between 15 and 100 J/g. Setting the mass of structure that undergoes crushing as the product of stroke l, cross-sectional area A, given by the product of thickness t and section length S, and density ρ:

$$\mathrm{SEA} = \frac{EA}{\rho \cdot A \cdot l} = \frac{\int F \cdot dl}{\rho \cdot t \cdot S \cdot l} \tag{4}$$

In the present study, density and thickness remain constant for all specimen geometries, thereby leaving as only variables of interest the section length S. Summary of the test results are reported in Table 3. For each of the specimen geometries listed, six test repetitions are performed, and the variation among these repetitions is captured via the Coefficient of Variation (CoV).

All specimens tested in this study crush in a stable manner, Figs. 7–11b, exhibiting frond formation and bending, particularly specimens II–V. The square tube, specimen I, exhibits an accordion-type of crushing, comprised of a succession of local segments folding on each other. It should be observed that the predominant failure mode at the corner is tearing fracture of the woven fiber tows (Fig. 10b), while in the flat segments it is lamina bending of the fronds. The load–displacement curves recorded show a relatively stable sustained force forming after the initiation of the crush, particularly for the corner element (Fig. 13). Stroke

Table 3
Summary of crush test results for all five specimen geometries.

Specimen no.	Shape	Peak force (kN)	Average crush force (kN)	Crush efficiency	Average SEA (J/g)	CoV (%)
I	Tube	39.9	23.8	1.68	36.9	10
II	Large channel	21.6	13.0	1.66	36.8	9
III	Small channel	17.1	10.7	1.60	42.7	3
IV	Small corner	7.5	4.9	1.53	62.3	11
V	Large corner	15.3	9.4	1.63	31.6	8

efficiency for all shapes varies between 1.38 and 1.65, which are right around the traditionally recommended value of 1.5 for efficient crushing. The load-stroke trace for one of the corner elements is shown in Fig. 14, from which the EA and SEA curves can be calculated. The results are normalized to their respective maximum values in order to be plotted in one chart. The EA curve is nearly perfectly linear, and the SEA curve shows a relatively smooth and rapid increase up to its horizontal asymptotic value (in a fashion similar to what in metals would be an elastic–perfectly plastic behavior). Similar curves can be obtained for all other geometries, but are not shown. Load–displacement curves are repeatable, and the Coefficient of Variation (CoV) in measured SEA varies between 3% and 11% between the five geometries, which is reasonable.

In general, it can be seen from Fig. 15 that the small corner element exhibits a much higher SEA than the other specimens, followed by the small and large C-channels, the square tube and, lastly, the large corner element. The small corner, exhibiting the least amount of flat segments in its cross-section, is therefore the most efficient in dissipating energy per unit mass of material crushed, and this can be attributed to the tearing failure mechanism observed. On the other hand, the large corner is the least efficient, exhibiting the most amount of flat segments in its cross-section, and this can be attributed to the frond bending failure mechanism observed. Fig. 16 shows the variation of SEA for all five shapes (denoted SEA_i, where i = I–V) normalized to the SEA of the corner element (denoted as SEA_{IV}) as it varies as a function of ΔS, which is given by Eq. (2):

$$\frac{SEA_i}{SEA_{IV}} = f(\Delta S) \tag{5}$$

It is clear from the plot that the SEA of the sections tested, for the material form and lay-up at hand, decreases linearly with increasing total length of flat segments.

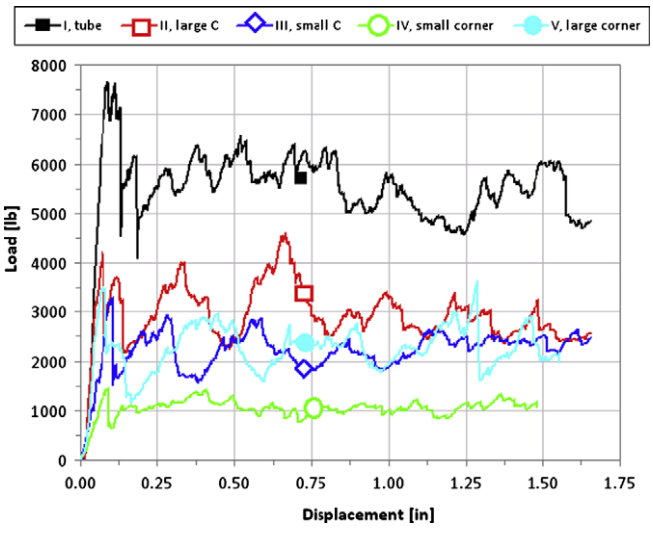

Fig. 13. Typical load–displacement curves for all five shapes considered.

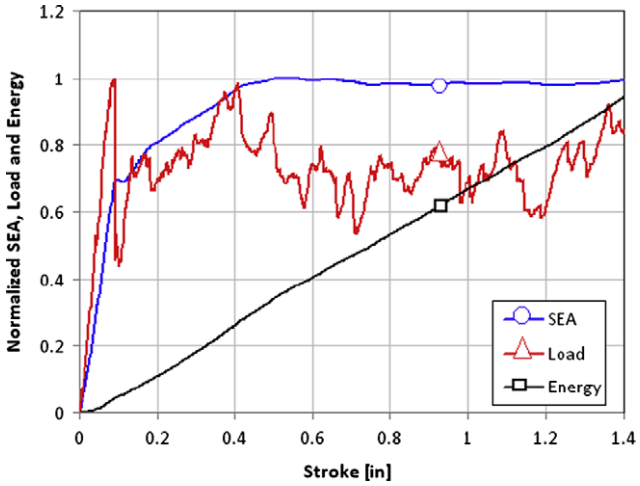

Fig. 14. Example of normalized load, energy absorbed (EA) and SEA vs. stroke curves for the corner element, specimen IV.

4. Discussion

The SEA_i for each shape can be subdivided into two components, one associated with the corner detail, obtained from testing a corner element and denoted SEA_{IV}, and one associated to the remaining flat segments, and denoted SEA_f. These SEA contributions are weighed based on the ratio of the lengths of corner detail (S_{IV}) with respect to the total length of the section (S_i), and of the remaining flat segments (ΔS) with respect to the total length of the section (S_i):

$$SEA_i = \left(\frac{S_{IV}}{S_i}\right) SEA_{IV} + \left(\frac{\Delta S}{S_i}\right) SEA_f \tag{6}$$

If Eq. (6) is solved for the unknown value of SEA_f since all other quantities are either known or can be measured experimentally, it is possible to extrapolate the in situ value of the SEA associated with flat sections, like the ones that form the fronds observed in splaying failure. The average value obtained this calculation is SEA_f = 16.3 J/g (Fig. 17), which is much lower than the average SEA_{IV} = 62 J/g recorded during the crushing of the corner elements. Although there is evident variation in the results, it is consistent with the CoV measured between repetitions. In conclusion, although the corner element exhibits a higher measured SEA than any of the other shapes tested, the contribution of the flat sections cannot be neglected.

To validate these observations, a limited number of tests are performed using the special fixture developed by the authors [7]. As seen in Fig. 18, the SEA measured using the flat specimen varies greatly according to the value of unsupported height used. For 0 in. (0 mm) of unsupported height, which means for a fully constrained specimen as in the case of the original NASA fixture, the SEA measured greatly overestimates the real SEA of the material. As the unsupported height is increased to 0.125 in. (3.18 mm), the SEA quickly drops, and eventually for 0.25 in. (6.35 mm) and greater

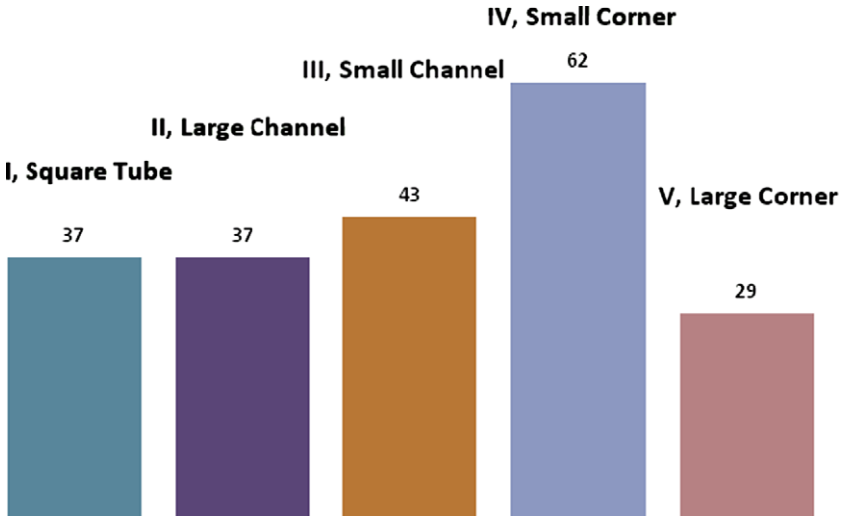

Fig. 15. Summary of average SEA results in J/g for all five specimens tested.

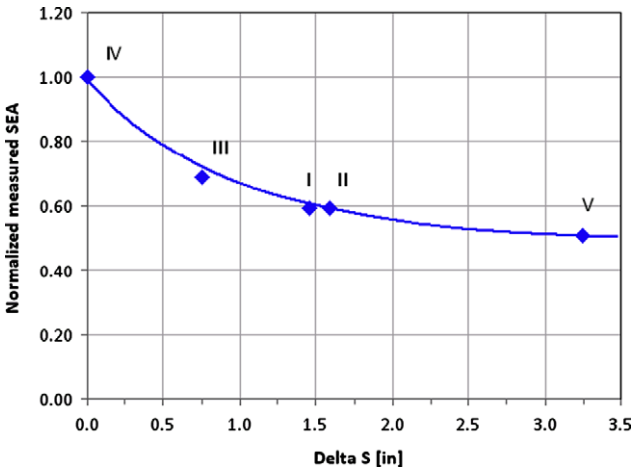

Fig. 16. SEA for geometries I–V, normalized against the SEA of the corner element IV, and plotted against the total length of flat segments in the cross-section.

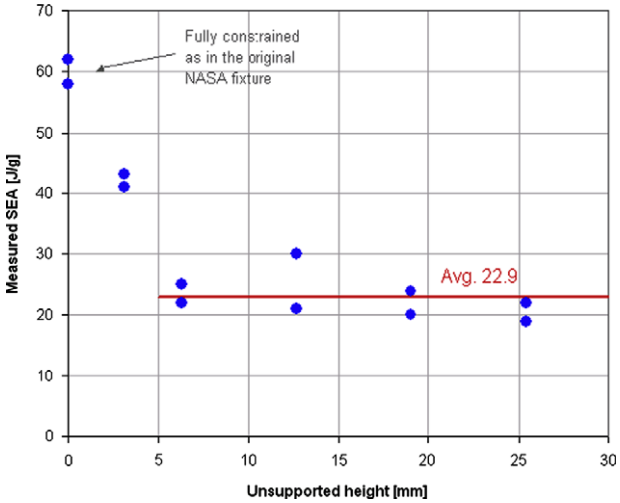

Fig. 18. SEA of flat specimen as a function of unsupported height, measured using the fixture in Fig. 12 and described in [7].

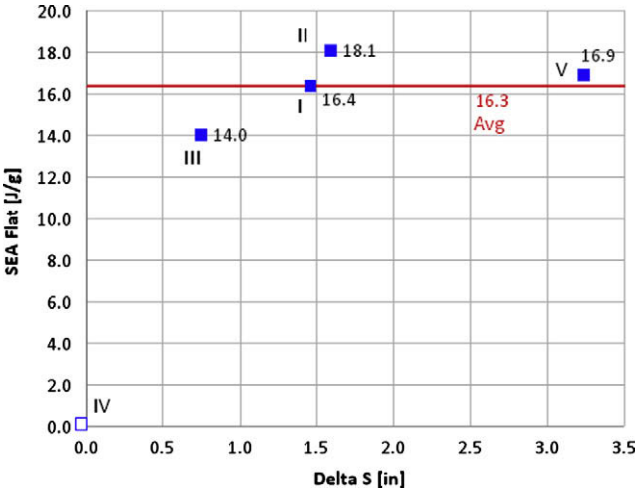

Fig. 17. Extrapolated in situ SEA of flat segment, from Eq. (6), plotted against the total length of flat segments in the cross-section.

it reaches an asymptotic value of 22.9 J/g. Although slightly higher, this value is relatively close to the one determined in situ through Eq. (6). At the same time, it suggests that the flat plate test methodology tends to overestimate the SEA, possibly due to unknown fixture effects, such as friction. A typical flat specimen before testing is shown in Fig. 19, left, where the sawtooth trigger is clearly visible. A typical post-crush specimen is shown in Fig. 19, right, for an unsupported height of 0.5 in. (12.5 mm).

From the study it is possible to note that the degree of curvature greatly influences the energy absorption behavior: the more contoured the specimen cross-section, the higher the energy dissipated per unit mass of material. This observation becomes evident in Fig. 20, which plots the variation of SEA with respect to the dimensionless index ϕ, which is an indicator of the degree of curvature of the cross-section, and is given by:

$$\phi = \frac{l}{S_i} = \frac{\pi \cdot r}{2 \cdot S_i} \tag{7}$$

where l is the arc length, given by the product of the radius r and the angle $\pi/2$, and S_i is length of the cross-section influenced by the corner, as defined in Eq. (1).

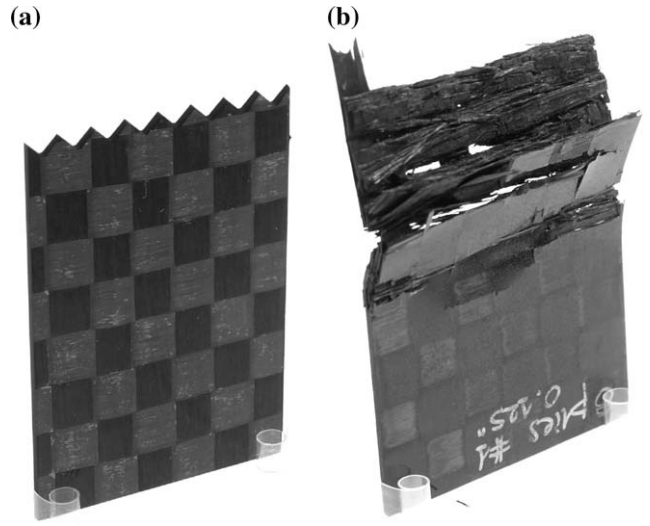

Fig. 19. (a, b) Flat specimen, before crushing showing the saw-tooth trigger (a), and after crushing (b) at 12.5 mm of unsupported height.

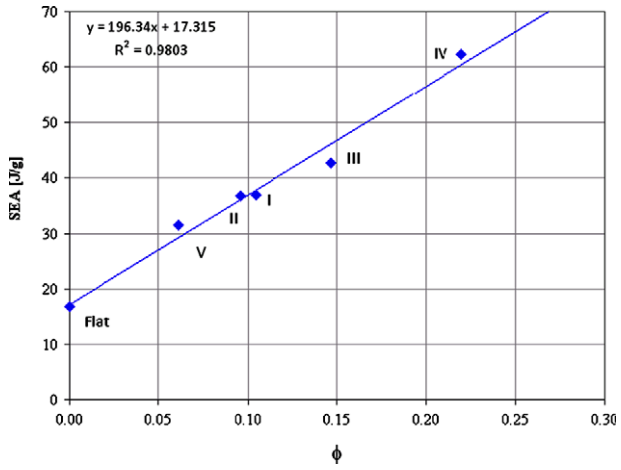

Fig. 20. SEA variation with ϕ, which is an indicator of curvature per unit length of cross-section for all specimens tested.

Segments of cross-section characterized by changes in curvature, such as corners, are much more efficient in absorbing energy than sections with long flat segments, as shown in Fig. 20, where there appears to be a linear trend between SEA and the dimensionless parameter ϕ.

This in turn implies that if a test specimen, such as a small corner element, is used to measure the SEA, it may overestimate the energy dissipation of a structure comprised of corners and flat segments. At the same time, ignoring the contribution of these flat segments and considering the SEA of the corner details alone will underestimate the energy dissipation of such structure. Therefore the results support the development of one or more test methods to measure the SEA for flat plate specimens, and for portions of structures characterized by changes in curvature. The results also support the concept that crushing is a not just a material property but a combined material/structure property.

5. Conclusions

Starting from a baseline of a fabric prepreg square tube, specimens with different geometric characteristics have been successfully crushed, including C-channels and corner elements of varying cross-section lengths. Laminate thickness, material system, manufacturing process, and test methodology used are kept constant throughout the study to specifically isolate the effects of cross-section geometry on the crush behavior for each specimen. It is found that for the material and lay-up considered, the small corner element is the most efficient in absorbing energy per unit mass compared to those with longer flanges, particularly the square tube. The more contoured the specimen (i.e. the least amount of flat segments), the higher the measured SEA. Fiber tensile fracture and tearing at the corners of a square tube is responsible for the vast percentage of the energy absorbed, while frond formation and splaying of the large flat segments is responsible for a much lower percentage. In order to maximize the energy absorption it becomes fundamental to suppress delamination propagation and to minimize formation of large fronds while promoting fragmentation as failure mechanism. In the attempt to standardize test methodologies for composite crush energy absorption, it becomes important to acknowledge that at the SEA for curved sections and flat plate sections are different and it is necessary to generate at separate SEA values in order to capture the crush behavior of geometrically complex structures.

Acknowledgments

The authors would like to express their gratitude to the Dr. Larry Ilcewicz, Mr. Curt Davies and Mr. Allan Abramowitz (Federal Aviation Administration) for sponsoring the research. They would also like to thank the Crashworthiness Working Group of the CMH-17 (formerly known as MIL-17 Handbook). Leslie Cooke and Andrea Dorr (Toray Composites of America) for supplying the material and specimens used in the study, and undergraduate student Enrique Gally Galgana for helping with the testing and graphics.

References

[1] Carruthers JJ, Kettle AP, Robinson AM. Energy absorption capability and crashworthiness of composite material structures: a review. Appl Mech Rev 1998;51:635–49.
[2] Browne A, Johnson N, Botkin M. Dynamic crush response of RTM crash boxes. In: ASC 24th technical conference, Memphis, TN; September 2008.
[3] Composite materials handbook (CMH-17). Crashworthiness and energy management, vol. 3 [chapter 13, rev. G]. West Conshohocken, Pennsylvania, USA: ASTM International; 2009.
[4] Johnson A. Determination of composite energy absorption properties. In: Proceedings of the 50th MIL-HDBK-17 coordination meeting – Crashworthiness Working Group, Chicago, IL; July 2006.
[5] Bolukbasi AO, Laananen DH. Energy absorption in composite stiffeners. Composites 1995;26(4):291–301.
[6] Feraboli P. Development of a corrugated test specimen for composite materials energy absorption. J Compos Mater 2008;42(3):229–56.
[7] Feraboli P. Development of a modified flat plate test specimen and fixture for composite materials crush energy absorption. J Compos Mater. in press.
[8] Lavoie JA, Morton J. Design and application of a quasi-static crush test fixture for investigating scale effects in energy absorbing composite plates. NASA CR 4526; July 1993.
[9] Jackson K, Morton J, Lavoie J, Boitnott R. Scaling of energy absorbing composite plates. J AHS 1994;39(1):17–23.
[10] Tomblin J, Sherraden J, Seneviratne W, Raju KS. A-basis and B-basis design allowables for epoxy-based prepreg Toray T700SC-12K-50C/#2510 plain weave fabric. In: AGATE-WP3.3-033051-131; September 2002.
[11] T700SC 12K/2510 plain weave fabric. Composite materials handbook (CMH-17), vol. 2 [chapter 4.2.38, rev. G.]. West Conshohocken, Pennsylvania, USA: ASTM International; 2009.